Numerical simulation of supercontinuum generation based on the active nonlinear fiber*

JIA Cai-ping (贾彩萍) **and WANG Chun-can** (王春灿)**

Key Laboratory of All Optical Network and Advanced Telecommunication Network, Ministry of Education, Institute of Lightwave Technology, Beijing Jiaotong University, Beijing 100044, China

(Received 11 April 2020; Revised 27 May 2020)

The supercontinuum (SC) generation (SCG) based on the active nonlinear fiber has attracted much attention due to its advantages in the energy amplification and spectral broadening of the output pulses. The active step-index single-mode fiber is proposed for the SCG. A flat normal-dispersion profile ranging from 1 240 nm to 2 550 nm can be obtained by tuning the germanium (Ge) concentration and core size, where the values of the dispersion slope are between −0.01 ps/nm^2/km and 0.05 ps/nm^2/km. Furthermore, the output pulse from the 5 m Er-doped normal-dispersion fiber (NDF) with g_0=9 m^{-1} has a peak power of 2.8 kW and a 20 dB spectral bandwidth of 507 nm ranging from 1 262 nm to 1 769 nm by using the 1 550 nm and 1 ps Gaussian pulse with a peak power of 10 kW as the pumping source.

Document code: A **Article ID:** 1673-1905(2021)03-0149-6

DOI https://doi.org/10.1007/s11801-021-0063-0

SCG in the normal-dispersion active fiber refers to the process of spectral broadening due to the combined effects of fiber dispersion, gain and nonlinearity, which mainly includes self-phase modulation (SPM), four-wave mixing (FWM) and stimulate Raman scattering (SRS). Since the SC laser sources based on the optical fibers have many advantages such as high beam quality, easy maintenance and compact structure, they can be employed in the optical coherence tomography[1], spectroscopy[2] and biomedical[3], etc. Recently, the supercontinuum generation (SCG) based on the active highly nonlinear fiber has attracted much attention due to the combined function of energy amplification and spectral broadening. The SCG can be obtained by using the active-type fibers such as the photonic crystal fibers (PCFs)[4,5], ZBLAN (ZrF4-BaF2-LaF3-AlF3-NaF) fibers[6-8] and double cladding fibers[9,10]. For example, the Yb-doped PCF can be used for the SCG, where the spectral bandwidth can reach up to 400 nm[4]. Moreover, the output pulse from the Ho-doped ZBLAN exhibits a broad spectrum ranging from 2 030 nm to 2 900 nm. However, the ZBLAN fiber based on the soft glass cannot be handled and spliced as straight forward as the silica fiber[6]. The Yb-doped double-cladding silica fiber amplifier can generate the high-power SC light with 10 dB spectral bandwidth of 1 130 nm, where the SCG system is an all-fiber compact structure[9].

In this paper, the active normal-dispersion fiber (NDF), by which the propagating pulses can be amplified and spectrally broadened, is proposed based on the heavily Ge-doped silica. Additionally, compared with the PCFs and ZBLAN fibers, the step-index NDF has a more simple structure, which is helpful to the fabrication and fusion splice of the optical fiber. The properties of the active NDF the dispersion, nonlinear parameter, loss and gain, are discussed. Moreover, the evolution of propagating pules along the fiber are numerically simulated and analyzed in the spectral and temporal domains.

Fig.1 shows the schematic diagram of the SCG configuration, where the initial pulses (blue line) undergo the combined effects of dispersion, gain and nonlinearity interactions through the active NDF. The fiber core made of Ge-doped silica is doped by erbium ion for obtaining gain, which is surrounded by the pure-silica cladding. The parameters n_1 and n_2 represent the refractive indices of Ge-doped[11] silica and pure silica[12], which can be calculated using:

$$n_1^2(\lambda)-1=\sum_1^3\frac{\left[SA_i+X(GA_i-SA_i)\right]\lambda^2}{\lambda^2-\left[SI_i+X(GI_i-SI_i)\right]^2}, \tag{1}$$

$$n_2^2=1+\frac{0.696\,166\,3^2}{\lambda^2-0.068\,404\,3^2}+\frac{0.407\,942\,6^2}{\lambda^2-0.116\,241\,4^2}+\frac{0.897\,479\,4^2}{\lambda^2-9.896\,161^2}, \tag{2}$$

where SA_i, SI_i, GA_i, and GI_i are the Sellmeier coefficients for the Ge-doped silica. X is the Ge concentration in mol%[12,13]. Moreover, the profiles of the group velocity dispersion (GVD) for the fiber can be tailored by tuning the core radius r_{core} and the Ge concentrate X.

As shown in Fig.2(a) and (b), the curves of Ge-doped silica material dispersion and refractive indices are calculated as functions of the Ge concentrate X, respectively.

* This work has been supported by the National Natural Science Foundation of China (No.61575018).

** E-mail: chcwang@bjtu.edu.cn

It can be seen that the material dispersion curve has a red shift with an increase of the Ge concentrate. For this reason, a flat normal dispersion profile can be obtained by tuning the wave-guide dispersion for the heavily Ge-doped silica fiber.

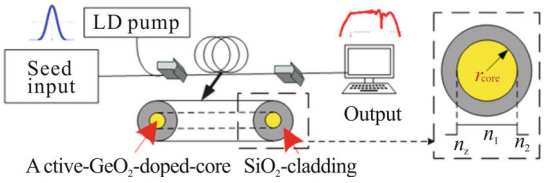

Fig.1 Schematic illustration of the SCG based on an active NDF with the cross section shown on the right side, where r_{core} represents the radius of the core, n_1 and n_2 are the refractive indices for the GeO$_2$-doped silica and pure silica, respectively

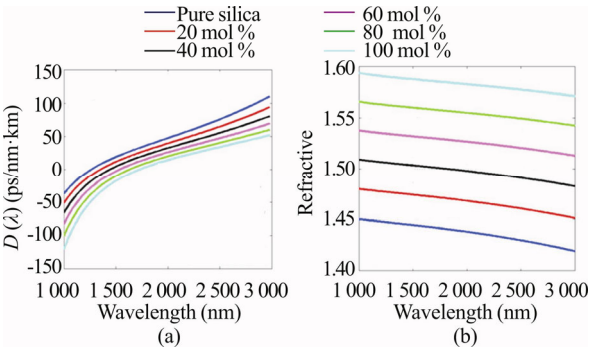

Fig.2 The curves of material (a) dispersion and (b) refractive indices of the Ge-doped silica and pure silica

The GVD parameter $D(\lambda)$ can be written as

$$D(\lambda) = -\frac{\lambda}{c}\frac{\mathrm{d}^2 n_{\mathrm{FM}}(\lambda)}{\mathrm{d}\lambda^2}, \tag{3}$$

where n_{FM} is the effective index of the fundamental mode (FM) at the operating wavelength λ. The nonlinearity parameter $\gamma(\lambda)$ can be defined as[14]

$$\gamma(\lambda) = \frac{2\pi}{\lambda}\frac{\int\int_{-\infty}^{\infty} n_2(x,y)\left|F(x,y)\right|^4 \mathrm{d}x\mathrm{d}y}{\left(\int\int_{-\infty}^{\infty}\left|F(x,y)\right|^2 \mathrm{d}x\mathrm{d}y\right)^2}, \tag{4}$$

where $n_2(x, y)$ is the nonlinear-index coefficient, and $F(x, y)$ is the modal intensity distribution of the fiber mode. The values of n_2 of Ge-doped silica and pure silica are $(2.16+0.033X)$[15,16] and 2.2[16] with the unit of 10^{-20} m^2/W, respectively.

For the active NDF with the normalized frequency V<2.404 8, the nonlinear parameters and GVD in the wavelength range from 1 000 nm to 3 000 nm are shown in Fig.3 with different values of X and r_{core}. When the values of X increase from 20 mol% to 100 mol%, the ZDWs for the active NDFs shift toward longer wavelength sides. It can be seen that the fiber has the relatively flat normal-dispersion profile near the wavelength of 1 550 nm (−12.46 ps/(nm·km)) when X=40 mol% and r_{core}=1.4 m. Furthermore, the corresponding dispersion slope varies from −0.01 ps/nm^2/km to 0.05 ps/nm^2/km in the wavelength range of 1 240—2 550 nm (blue curve) shown in Fig.3(b). Fig.3(c) shows that the nonlinear parameters increase with increasing the X due to a decrease of the effective mode areas A_{eff}. For example, the nonlinearity parameters increase from 0.008 W^{-1}/m to 0.036 W^{-1}/m at the wavelength of 1 550 nm when increasing X from 20 mol% to 100 mol%.

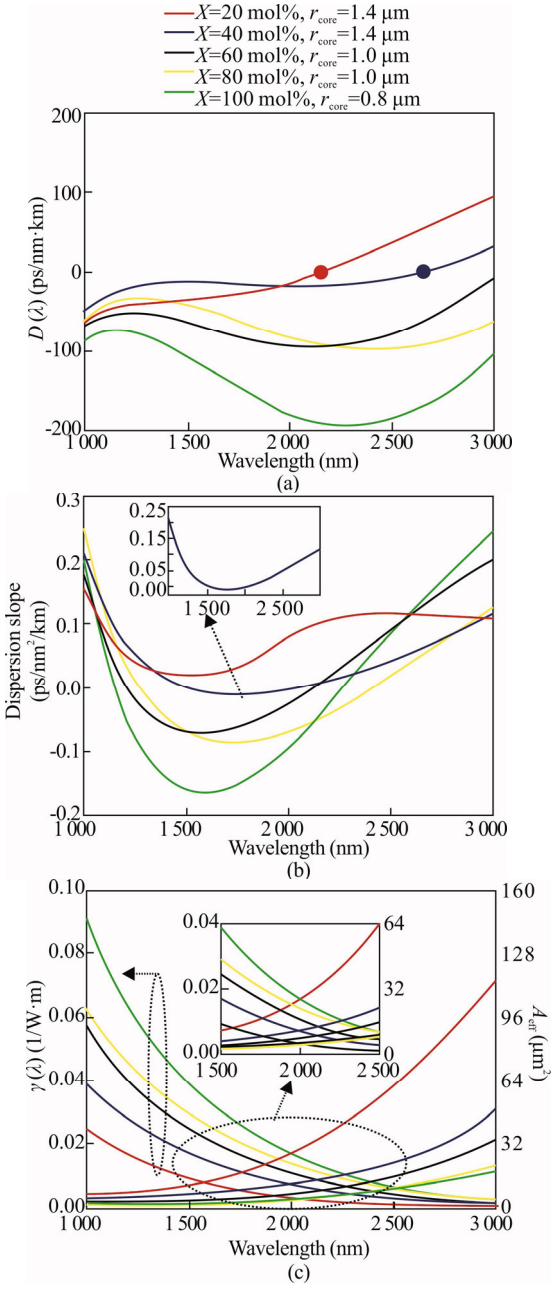

Fig.3 The curves of (a) GVD, (b) the dispersion slope, and (c) the nonlinear parameter $\gamma(\lambda)$ (left) with effective mode area A_{eff} (right) for different values of X and r_{core}

The total loss L of the optical mode includes both confinement loss L_{C} and the absorption loss L_{A} in the fiber, which can be expressed by[14]

$$L_{\mathrm{C}}(\lambda) = \frac{20}{\ln(10)}\frac{2\pi}{\lambda}\mathrm{Im}(n_{\mathrm{eff}}), \tag{5}$$

$$L_{\mathrm{A}} = \Gamma^{\mathrm{core}}(\lambda)\times\alpha_{\mathrm{GeO_2}} + \Gamma^{\mathrm{cladding}}(\lambda)\times\alpha_{\mathrm{SiO_2}}, \tag{6}$$

where $\mathrm{Im}(n_{\mathrm{eff}})$ represents the imaginary part of the effective

index of the modes. The parameters $\Gamma^{\text{core}}(\lambda)$ and $\Gamma^{\text{cladding}}(\lambda)$ are the fractions of the mode intensity in the core and cladding. The absorption losses in the Ge-doped silica and pure silica are α_{GeO2} and α_{SiO2}, respectively.

In addition, the gain characteristic is closely related to the absorption spectrum $\alpha_{\text{A}}(\lambda)$ and gain spectrum $g(\lambda)$ for the Er-doped fibers, which are given by[17]

$$\alpha_{\text{A}}(\lambda)=\Gamma^{\text{core}}(\lambda)\sigma_{\text{a}}(\lambda)N_{\text{t}}, \tag{7}$$

$$g(\lambda)=\Gamma^{\text{core}}(\lambda)\sigma_{\text{e}}(\lambda)N_{\text{t}}, \tag{8}$$

where $\sigma_{\text{a}}(\lambda)$ and $\sigma_{\text{e}}(\lambda)$ are the absorption and emission cross sections at wavelength λ, respectively. N_{t} refers to the erbium concentration at the doping region.

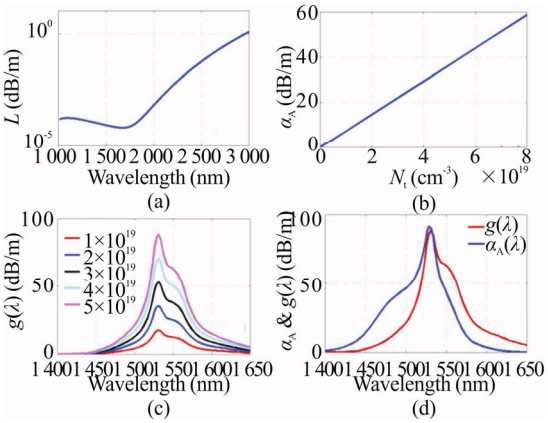

Fig.4 (a) The total loss *L*; (b) The absorption α_{A} as a function of N_{t} with $\sigma_{\text{a}}=1.879\times10^{-25}$ m^2[18] and $\Gamma^{\text{core}}=0.9$ in the wavelength of 980 nm; (c) The gain spectra $g(\lambda)$ for different values of N_{t}; (d) The absorption spectra $\alpha_{\text{A}}(\lambda)$ & gain spectra $g(\lambda)$ with $N_{\text{t}}=5\times10^{19}$ cm^{-3} as function of wavelength, where X=40 mol% and r_{core}=1.4 m

As shown in Fig.4(a), the total losses L are much less than 1 dB/m at most wavelengths ranging from 1 000 nm to 2 500 nm. For the Er-doped NDF, the pumping source is the 980 nm single-mode laser diodes. As a result, the absorption of the pump α_{A} (λ= 980 nm) increases linearly with the doping concentration show in Fig. 4(b), which can reach to 36.72 dB/m when $N_{\text{t}}=5\times10^{19}$ cm^{-3}. The values of gain increase with an increase of N_{t}, especially for the gain peak near the wavelength of 1 530 nm in Fig.4(c). Furthermore, the values of gain $g(\lambda)$ near the wavelength of 1 550 nm are more than 60 dB/m when $N_{\text{t}}=5\times10^{19}$ cm^{-3}, as shown in Fig.4(d). These results indicate that the active NDF can provide high enough gain in the 1 550 nm window when the fiber is heavily doped with erbium irons.

The generalized nonlinear Schrödinger equation (GNLSE) is used to describe the evolutions of the propagating pulses along the active NDF, which can be written by[20]

$$\frac{\partial A}{\partial z}+\left(\frac{\alpha}{2}-\frac{g}{2}\right)A+\sum_{n=2}^{\infty}\frac{\mathrm{i}^{n-1}}{n!}\beta_n\frac{\partial^n A}{\partial T^n}=$$
$$\mathrm{i}\gamma\left(1+\frac{\mathrm{i}}{\omega_0}\frac{\partial}{\partial T}\right)\left[A(z,T)\int_0^{\infty}R(t')\left|A(z,T-t')\right|^2\mathrm{d}t'\right], \tag{9}$$

where $A(z, T)$ represents the slowly varying pulse envelope function of the optical radiation field in time domain. The time derivative term on the right-hand side models the dispersion of the nonlinearity, which is associated with the effects of self-steepening and optical shock formation, characterized by a time scale $\tau_{\text{shock}}=1/\omega_0$. In this paper, the initial pulse is set to be a Gaussian pulse, i.e., $A(0,T)=\sqrt{P_0}\quad\exp(-T^2/2T_0^2)$, where $T_0=T_{\text{FWHM}}/\sqrt{2\ln 2}$; T_{FWHM} is the full width at half-maximum pulse duration, and peak power P_0 can be obtained by $P_0=0.94E_0/T_{\text{FWHM}}$, where E_0 is the pulse energy. α is the loss, β_n is the dispersion coefficients, and γ is the nonlinear parameter. The gain g is given by[20,21]

$$g=\frac{g_0}{1+E_{\text{pulse}}/E_{\text{sat}}+(\omega-\omega_0)^2/\Delta\omega_{\text{g}}^2}, \tag{10}$$

where g_0 is small-signal gain at the center wavelength of 1 550 nm related to the doping concentration, E_{pulse}, E_{sat} and $\Delta\omega_{\text{g}}$ are the instantaneous pulse energy, saturation energy, and gain bandwidth, respectively. The nonlinear response function $R(T)=(1-f_R)\delta(T)+f_R h_R(T)$ includes both instantaneous and delayed Raman contributions. f_R is the fractional contribution of the delayed Raman response to nonlinear polarization, which is given by 0.22. The Raman response term is given by[19]

$$h_R(T)=\frac{\tau_1^2+\tau_2^2}{\tau_1\tau_2}\exp(-T/\tau_2)\sin(T/\tau_1), \tag{11}$$

where τ_1 and τ_2 is related to the frequency of the "phonon" and the attenuation of the network of vibrating atoms, respectively. For silica-based fiber, the value of τ_1 and τ_2 is 12.2 fs and 32 fs, respectively.

The dispersion length and the nonlinear length are $L_{\text{D}}=T_{\text{FWHM}}^2/|b_2|$ and $L_{\text{NL}}=1/\gamma/P_0$, respectively. b_2 is the second-order dispersion. Depending on the relative magnitudes of L_{D}, L_{NL}, and the fiber length L, either dispersion or nonlinear effects may dominate along the fiber. In this case, L_{NL}=0.007 m with P_0 = 10 kW. When T_{FWHM} = 0.1 ps and β_2 = 0.015 9 ps^2/m, the dispersion length L_{D} is 0.62 m. Since the value of L (1~5m) is much longer than L_{D} and L_{NL}, the spectral broadening of the propagating pulse results from the combined effects of the GVD and SPM. For the case of T_{FWHM} are 0.5 ps and 1 ps, the L_{D} are 15.72 m and 62.89 m. As a result, the SPM effect dominates the process of the pulse evolution because L is much shorter than L_{D}.

As shown in Fig.5, the output pulses show broader spectra and higher peak powers when the fiber has a flat normal dispersion profile with relatively low absolute value of the GVD at 1 550 nm. For example, the absolute values of GVD at 1 550 nm are 12.46 ps/(nm·km), 68.16 ps/(nm·km) and 45.07 ps/(nm·km) when X=40 mol%, 60 mol% and 80 mol%, and the spectral bandwidth (at the 20 dB level) can reach 489 nm, 243 nm and 366 nm with the peak powers of 2.05 kW, 0.76 kW and 0.89 kW when z=5 m, respectively. Consequently, the values of X and r_{core} are taken to be 40 mol% and 1.4 μm in the following discussions. The parameters used in the simulation can be seen in Tab.1.

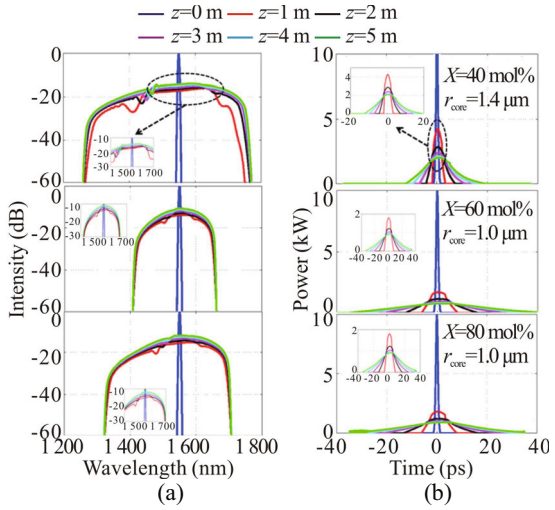

Fig.5 The output pulses from the active NDFs with z=0 m, 1 m, 2 m, 3 m, 4 m and 5 m for different values of X and r_{core} in (a) spectral and (b) temporal domains (For the initial Gaussian pulse, T_{FWHM}= 1 ps, g_0 = 6 m^{-1} and P_0 = 10 kW)

Tab.1 The parameters used in the simulation

Fiber parameters	Value	Input pulse parameters	Value
X (mol%)	40	T_{FWHM} (ps)	0.1—1
r_{core} (μm)	1.4	P_0 (kW)	10
γ (W^{-1}·m^{-1})	0.015	z (m)	0—5
GVD (ps/(nm·km))	−12.46	g_0 (m^{-1})	0—9
Loss (dB·m^{-1})	<1	λ_0 (nm)	1550

In Fig.6, it can be seen that increasing the value of g_0 can lead to spectral broadening of the output pulses. When the values of g_0 are 0 m^{-1}, 3 m^{-1}, 6 m^{-1} and 9 m^{-1}, the spectral widths of the output pulses at 20 dB level are 455 nm, 472 nm, 489 nm and 507 nm, and the corresponding pulse energies of the output pulses are 10.1 nJ, 19.5 nJ, 29.2 nJ and 39.5 nJ, respectively. Consequently, the active NDF offers a degree of freedom for broadening the spectral bandwidth and increasing the temporal intensity of the output pulses by tuning the parameter of g_0.

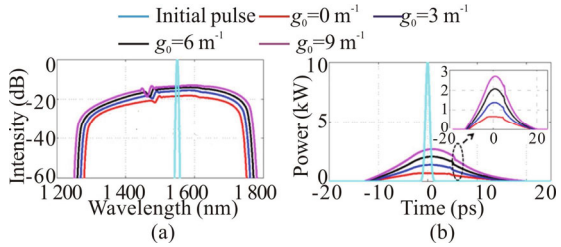

Fig.6 The output pulses from the active NDFs for different g_0 in (a) spectral and (b) temporal domains when z=5 m (For the initial Gaussian pulse, T_{FWHM}=1 ps and P_0=10 kW (10.6 nJ pulse energy))

Furthermore, Figs.7 and 8 show that the evolution of the propagating pulses in the spectral and temporal domains in the cases of g_0=9 m^{-1} (active fiber case) and 0 m^{-1} (passive fiber case) with a 1-ps input pulse. As shown in Fig.7(c) and (d), Fig.8(c) and (d), during the initial stage of pulse evolution, new frequency components can be created in the vicinity of the wavelength 1 550 nm due to the self-phase modulation (SPM). With a further propagation, the spectra exhibit significant broadening on the short wavelength sides due to the onset of optical wave breaking (WB) in the normal-dispersion regimes. The spectral energy is transferred from the pump wavelength regime into spectral wings via the effects of four wave mixing (FWM) induced by WB[12]. In both cases, as shown in Fig.7(a) and Fig.8(a), the spectral bandwidths of the propagating pulses show nearly linear increases with z at the early stage of pulse evolution, and then becomes saturated when z>2.5 m because of the decreases of the peak powers of the pulses. In addition, Fig.7(e) and Fig.8(e) shown the output spectra in the cases of g_0=9 m^{-1} and g_0=0 m^{-1} can be broadened to 507 nm (1 262—1 769 nm) and 455 nm (1 287—1 742 nm) at 20 dB level, respectively. In Fig.7(b) and Fig.8(b), it is worth noting that the pulses at the end of the fiber remain a nearly linear chirp in temporal domain in both cases. Furthermore, as shown in Fig.7(f), the peak power of the pulse at the output end is 2.8 kW, which is more than 4 times higher than that of the passive fiber case in Fig.8(f). Consequently, the gain provided by the active fiber can compensate the losses so that when the propagating pulses exhibit spectral broadening due to the nonlinearity, and the pulse energies can also be increased at the same time.

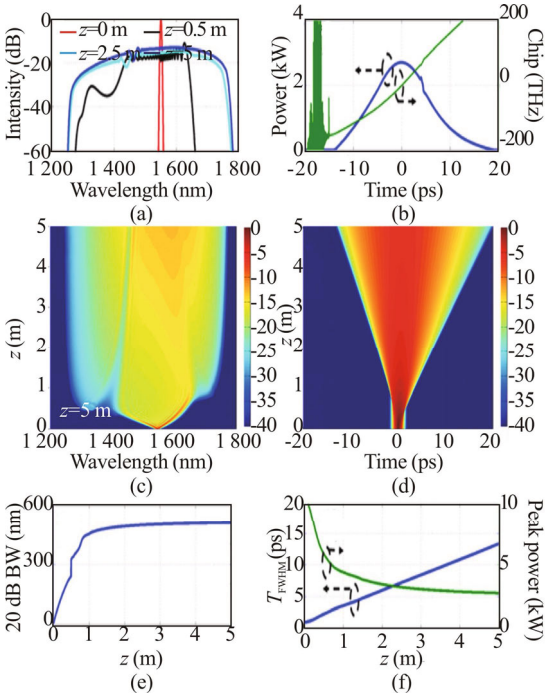

Fig.7 (a) The spectral intensities with different propagation distance z; (b) The temporal intensities with frequency-chirp profiles of the output pulses when z=5 m; The evolution of propagating pulses along the fiber in (c) spectral and (d) temporal domains when g_0=9 m^{-1}; (e) The 20 dB bandwidths and (f) the pulse widths T_{FWHM} (left) and peak power (right) of the propagating pulses as functions of z (For the initial Gaussian pulse, T_{FWHM}=1 ps and P_0=10 kW)

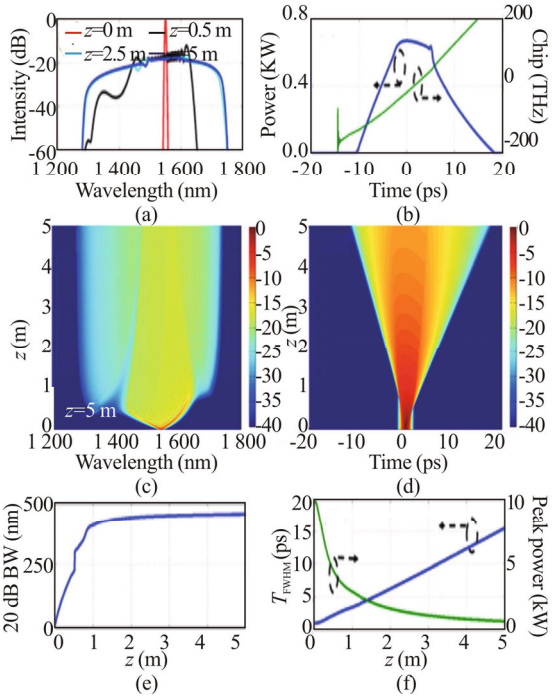

Fig.8 (a) The spectral intensities with different propagation distance *z*; (b) The temporal intensities with frequency-chirp profiles of the output pulses when *z*=5 m; The evolution of propagating pulses along the fiber in (c) spectral and (d) temporal domains when g_0=0 m^{-1}; (e) The 20 dB bandwidths and (f) the pulse widths T_{FWHM} (left) and peak power (right) of the propagating pulses as functions of *z* (For the initial Gaussian pulse, T_{FWHM}=1 ps and P_0=10 kW)

Furthermore, the 20 dB bandwidths and pulse energies of the propagating pulses are shown in Fig.9. It can be seen that the 20 dB bandwidths with z=5 m can reach 420 nm, 481 nm and 489 nm with pulse energies of 13.8 nJ, 21.2 nJ and 29.3 nJ, when T_{FWHM} = 0.1, 0.5 and 1 ps, respectively. When the initial T_{FWHM} is 0.1 ps, the spectral bandwidths decrease from 474 nm with z=0.2 m to 420 nm with z=5 m. The reason is that, as shown in Fig.10, the intensities of the frequency components in the gain spectrum are relatively higher than those of the frequency components on the blue and red sides because of the effect of optical amplification.

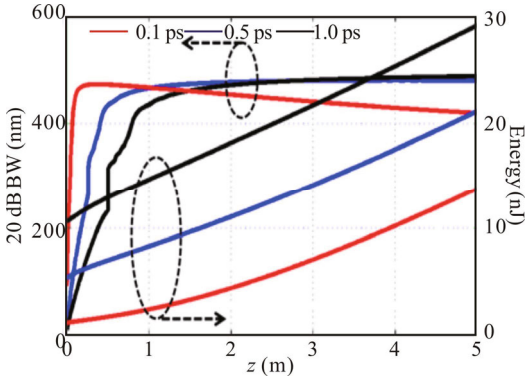

Fig.9 The 20 dB bandwidth (left) and the pulse energy (right) of the output pulses as the functions of the propagation distance *z* with g_0=6 m^{-1} for different T_{FWHM}

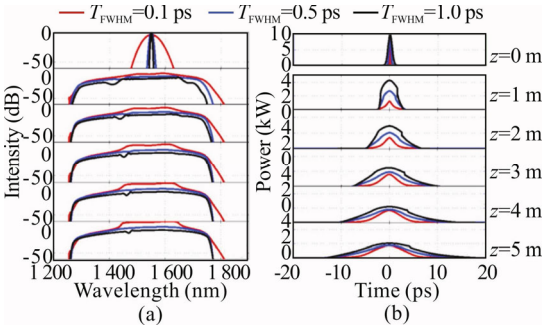

Fig.10 (a) The spectral evolution and (b) the intensity profiles in the temporal domain of the pulse along the active NDF with g_0=6 m^{-1} along the propagation distance *z* when initial pulse widths T_{FWHM}=0.1 ps, 0.5 ps and 1ps, where the other simulation parameters can be seen in Tab.1

In conclusion, the active fiber with a flat normal-dispersion profile in the spectral range of 1 240—2 550 nm is obtained by appropriate choice of the parameters. The corresponding values of the dispersion slope are between −0.01 ps/nm^2/km and 0.05 ps/nm^2/km. Furthermore, the numerical results show that the flat-top SC spectrum ranging from 1 262 nm to 1 769 nm can be realized by launching the pump pulse with the central wavelength of 1 550 nm in the fiber, where X=40 mol% and r_{core}=1.4 μm. At the same time, the propagating pulses along the active NDF can be amplified and preserve single-pulse state due to the effect of the normal dispersion.

References

[1] Wang Chen-yu , Kim J，Craig T J, Philip H W L and Alistair M, Journal of Near Infrared Spectroscopy **20**, 237 (2012).

[2] Andrew P L, Claire L. Greenwell, Jane Ireland, Emma R. Woolliams, Teresa M. Goodman, Agnieszka Bialek and Nigel P. Fox, Levick, Applied Optics **53**, 3508 (2014).

[3] Haohua T and Stephen A. Boppart, Laser & photonics reviews **7**, 628 (2013).

[4] Kwon Y, Park K, Hong S and Jeong Y, IEEE Journal of Quantum Electronics **53**, 1 (2017).

[5] Liu Zhao-lun and Zhang Chun-lan, Optik **161**, 172 (2018).

[6] Yang Lin-yong, Zhang Bin, Yin Ke, Zhao Yi-jun and Hou Jing, Journal of Lightwave Technology **36**, 3193 (2018).

[7] Yemineni S R, Lai W J and Alphones A, Optical Engineering **57**, 1 (2018).

[8] Yang Lin-yong, Zhang Bin, Wu Tian-yi, Zhao Yi-jun and Hou Jing, Optics Letters **43**, 3061 (2018).

[9] Aghayari E and Ghaleh K J, Applied optics **58**, 4020 (2019).

[10] Roman C, Jaouën Y, Tench R E and Delavaux J M, Optical Fiber Technology **54**, 102113 (2020).

[11] James W. Fleming, Applied Optics **23**, 4486 (1985).
[12] Wang Chun-can, Li Wei-min, Li Na and Wang Wen-quan, Optics & Laser Technology **88**, 215 (2017).
[13] Samoc A, Journal of Applied Physics **94**, 6167 (2003).
[14] Wang chun-can, Wang Mei-hui and Wu Jun, IEEE Photonics Journal **7**, 1 (2015).
[15] Boskovic A, Chernikov S V and Taylor J R, Optics Letters **21**, 1966 (1996).
[16] Yatsenko Y and Mavritsky A, Optics Letters **32**, 3257 (2007).
[17] Giles C R and Desurvire E, Journal of Lightwave Technology **9**, 271 (1991).
[18] Kang Qiong-yue, Lim Ee-Leong, Jung Yong-min, Jayanta K S, Francesco Poletti, Catherine Baskiotis, Shaif-ul Alam and David J. Richardson, Optics Express **20**, 20835 (2012).
[19] Agrawal G P, Nonlinear Fiber Optics & Applications of Nonlinear Fiber Optics, Beijing: Electronics Industry Press, 29 (2001). (in Chinese)
[20] Chong A, Wise F W and Renninger W H, Optics Express **14**, 10095 (2008).
[21] Huang Chun-yuan, Wang Cong, Shang Wei, Yang Nan, Tang Yu-long and Xu Jian-qiu, Scientific Reports **5**, 13680 (2015).